Smart Structures and Systems, *Vol. 22, No. 2 (2018) 139-150*
DOI: https://doi.org/10.12989/sss.2018.22.2.139

Design, analysis, and control of a variable electromotive-force generator with an adjustable overlap between the rotor and the stator

W.D. Zhu*[1], N. Goudarzi[2], X.F. Wang[1] and P. Kendrick[1]

[1]*Department of Mechanical Engineering, University of Maryland, Baltimore County, Baltimore, MD 21250, USA*
[2]*Mechanical Engineering Technology Program, Department of Engineering Technology and Construction Management, University of North Carolina at Charlotte, Charlotte, NC 28223, USA*

(Received May 2, 2017, Revised November 11, 2017, Accepted February 23, 2018)

Abstract. A variable electromotive-force generator (VEG), which is a modified generator with an adjustable overlap between the rotor and the stator, is proposed to expand the operational range of a regular generator through a simple and robust active control strategy. It has a broad range of applications in hybrid vehicles, wind turbines, water turbines, and similar technologies. A mathematical model of the VEG is developed, and a novel prototype is designed and fabricated. The performance of the VEG with an active control system, which adjusts the overlap ratio based on the desired output power at different rotor speeds for a specific application, is theoretically and experimentally studied. The results show that reducing the overlap between the rotor and the stator of the generator results in reduced torque loss of the generator and an increased rotational speed of the generator rotor. A VEG can improve the fuel efficiency of hybrid vehicles; it can also expand operational ranges of wind turbines and water turbines and harness more power.

Keywords: modeling; design; variable electromotive-force generator with an adjustable overlap between the rotor and the stator; hybrid vehicle; wind turbine; active control system

1. Introduction

While most of energy used in residential and commercial applications is provided by crude oil, natural gas, and coal, their environmental and sustainability issues have been drawing more concerns in recent decades. New technologies that use various types of renewable energy are being studied to address these issues and more efficiently expand the use of green energy sources. A variable electromotive-force generator (VEG) technology with a broad range of applications in hybrid vehicles, wind turbines, water turbines, and similar technologies is proposed and developed in this work.

The total power loss in an electric machine is caused by several different mechanisms: resistance of winding (copper loss), electrical current induced in the magnetic core (eddy current loss), and magnetic friction in the core (hysteresis loss) (Nasar and Boldea 1990). Only copper loss exists when the current in the winding does not change; all other losses fall to zero with the frequency. Eddy current loss can be minimized by choosing the magnetic core with lower electrical conductivity or by using laminations; hysteresis loss can be minimized by reducing the maximum magnetic flux density and the frequency, and by choosing materials with lower permeability such as permalloys (Bishop 2008). Figure 1 shows the torque drag versus the generator rotor speed in a synchronous machine [3]. A generator usually consists of three major components including the rotor, the stator, and the generator frame. While at the full overlap between the rotor and the stator, as in all regular generators, the torque drag rapidly increases with the rotor speed; at the minimum overlap between the rotor and the stator, as in the proposed generator technology, the torque drag has a slow increase with the rotor speed due to bearing friction. By changing the overlap between the rotor and the stator, power loss of a generator can be adjusted, which is the main motivation for developing the VEG technology.

Different machines with a variable electromotive-force/flux feature that allows flexibility in machine efficiency optimization throughout its working range have been studied by a number of researchers (Caricchi *et al.* 2001, Ferraro *et al.* 2006, Gaussens *et al.* 2013, Mbayed *et al.* 2012, Owen *et al.* 2011, Zhou *et al.* 2010). The variable flux can be obtained through mechanical adjustment, use of hybrid-excited machines with field coils, and other approaches that do not use specific mechanical adjustment or field coils (Gaussens *et al.* 2013, Mbayed *et al.* 2012, Owen *et al.* 2011).

The electric vehicle (EV) concept was introduced to reduce primary energy consumption and pollutant emission in transportation systems. New techniques have been studied to improve the performance and decrease pollutant emission of EVs. Hybrid EVs have been developed to address some drawbacks of EVs, mainly due to limited driving ranges and storage issues; they provide longer driving ranges with lower fuel consumption and pollutant emission (Bauman *et al.* 2000). Al-Adsani *et al.* (2009) studied new hybrid excitation synchronous machines that optimize the hybrid capability and provide a simpler control

*Corresponding author, Professor
E-mail: wzhu@umbc.edu

ISSN: 1738-1584 (Print), 1738-1991 (Online)

in storing power with a constant voltage. Crescimbii *et al.* (2005) proposed a compact permanent-magnet (PM) generator design that addresses some challenges such as the size and the cooling system of a hybrid EV generator. Rafiee *et al.* (2012) proposed a generator design using thermoelectric materials to improve the performance of a hybrid EV. Somayajula *et al.* (2009) studied variations and important design criteria in the design of energy storage systems of hybrid EVs. A VEG feature can be employed in different hybrid EV topologies with different generator types and materials, and storage systems. Caricchi *et al.* (2001) used a variable electromotive-force feature for an axial-flux PM machine in weakening the flux linkage to achieve a constant-power operation for the starter/alternator in an automotive application; however, it was achieved in a limited speed range. Del Ferraro *et al.* (2006) fixed this speed-range limitation by proposing an axial-flux PM machine with an extended speed range. Mbayed *et al.* (2012) proposed a hybrid excitation synchronous machine at which they used advantages of both the PM and wound rotor machines to reduce copper losses in electric vehicles. The electromagnetic torque adjustment can also be achieved in other ways; Chau *et al.* (2006) have done this regulation by weakening or strengthening the air-gap flux using small DC field current. Machines with mechanically adjusted magnetic fields provide a better torque density with less manufacturing and control strategy complexity compared with those with hybrid fields in series/parallel flux paths (Owen *et al.* 2011). Axial machines with rotor/stator displacements have shown better performance and less complexity among the machines with mechanically adjusted magnetic fields. Zhou *et al.* (2010) have proposed a variable flux motor to improve the motor efficiency at higher rotational speeds by mechanically weakening the magnetic field. Zepp *et al.* (2011) have done experimental studies on a brushless PM electric machine with a simpler design compared with the proposed motor by Zhou *et al.* (2010); the design improves fuel efficiency of a hybrid vehicle at low speeds by eliminating induced power loss in the generator. Emadi *et al.* (2005) studied operational characteristics of different topologies of hybrid electric vehicles from light duty passenger cars to heavy-duty buses. Williamson *et al.* (2006) showed advantages of a parallel hybrid drivetrain over a serial hybrid one, especially for city transit bus applications. Recently, Allison Transmission Inc. announced its H3000 hybrid propulsion system with a similar VEG feature for transit buses; an increase of 25-40% in miles per gallon and a similar percentage of reduction in CO_2 emission have been achieved in medium- to heavy-duty vehicles (Automotive World 2013). As a vehicle decelerates, the overlap between the rotor and the stator of the generator increases to generate electricity that can be stored in batteries or ultra-capacitors. As the vehicle accelerates, the overlap between the rotor and the stator of the generator goes back to its minimum to reduce the torque drag as shown in Fig. 1; the stored energy will be released and a vehicle can more smoothly and efficiently accelerate. With use of some concepts similar to the VEG feature, significant improvement in the efficiency of a hybrid vehicle and at the same time more reduction in global

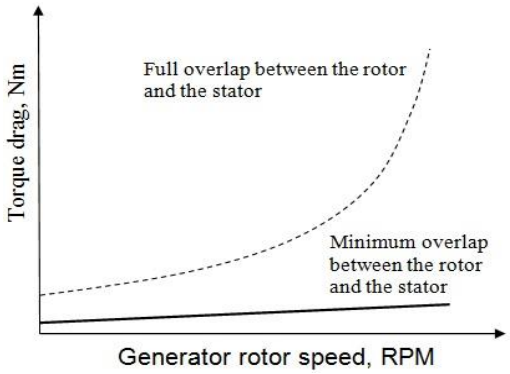

Fig. 1 Torque drag versus the generator rotor speed with minimum and full overlaps between the rotor and the stator

warming pollution have been noted by some researchers in industry.

Various types of renewable energy have been proposed and developed in recent decades; wind power has been drawing more interest and more rapidly improving its market share due to its advantages in terms of sustainability, environmental impacts, and being economical compared with other types of renewable energy (Goudarzi *et al.* 2014). Onshore/offshore wind turbines are used to convert the kinetic energy in wind into mechanical power, and generators convert the mechanical power into electricity for residential and commercial applications (Hau *et al.* 2006, Manwell *et al.* 2009). In the last few decades, wind turbines with different drivetrain topologies, such as direct-drive wind turbines with PM synchronous generators or electrically-excited synchronous generators, distributed drivetrains with multiple generators working all together, and single-stage drivetrains with medium-speed generators, have been developed to increase the maximum power capture, minimize the cost, and expand the use of wind turbines in both onshore and offshore applications (Bywaters *et al.* 2004, Chen *et al.* 2009, Deng and Chen 2010, Goudarzi and Zhu 2013, Li *et al.* 2006, Mikhail 2011). While state-of-the-art technologies such as high-temperature-superconducting generators with smaller size, better power quality, and higher reliability compared with conventional and recent technologies have been studied in recent years (Chen *et al.* 2005, Dubois 2004, Lewis and Muller 2007, Polinder *et al.* 2006, Schiferl *et al.* 2008), they are expensive to be used on commercial basis (Schiferl *et al.* 2008).

There are also other innovative solutions such as multiple-generator drivetrains with clutches that are still in the development phase (Goudarzi and Zhu 2013). On the other hand, wind turbines with doubly-fed-induction generators are still the market leader with more than 80% share on the market (Goudarzi and Zhu 2013). While power generation of a wind turbine is generally decided by its power curve, any improvement in the turbine component performance and efficiency can improve the system performance. A VEG feature can be employed in onshore/offshore wind turbines and water turbines with different drivetrain configurations; this feature can improve

turbine power curves and expand their operational ranges. At low input speeds, the overlap between the rotor and the stator can be adjusted to minimize the torque drag and keep the generator rotor spinning; it can be increased as the input speed increases to generate the maximum power. Goudarzi *et al*. (2012) used aerodynamics principles to study the performance of a wind turbine with a VEG feature; the study shows the possibility of expanding the operational range and increasing the efficiency of a wind turbine, especially in areas with high wind speed fluctuations and low annual mean wind speeds.

In this work, a novel VEG design to be used in a variety of applications such as hybrid vehicles, wind turbines, water turbines, and so on is presented to expand the operational range of a regular generator by adjusting the overlap between the rotor and the stator through a simple and robust active control strategy. A mathematical model of the VEG is developed, a prototype is designed and fabricated, and an active control system for adjusting the overlap between the rotor and the stator based on the desired output power at different input speeds is developed. Theoretical analysis and electromagnetic principles together with experimental tests are employed to better understand the changes in the electromotive force (EMF) and the generator rotor speed with the overlap between the rotor and the stator, and to improve the generator output power. The stability of the control system is studied and the control results from the prototype are presented. Hence, this scalable VEG design proposes a more reliable, simpler, and efficient performance (Zepp 2011), and provides a stable output compared with the similar design used for a hybrid vehicle (Zepp 2011).

2. Mathematical modeling of the VEG

The fundamental operation of a synchronous generator or other electric machines can be understood by using Maxwell's equations. The magnetic flux Φ is defined as the integration of the cross product of the magnetic field flux density B and the differential cross sectional area vector *dA*

$$\Phi = \int B \times dA \tag{1}$$

The induced voltage is described by applying Faraday's law of induction on a conductor moving in a static magnetic field (Wentworth 2005)

$$E = -N\frac{d\Phi}{dt} = -NB\frac{dA}{dt} = -NBl_f\frac{ds}{dt} = -NBl_f v \tag{2}$$

where E is the induced voltage or the EMF that is proportional to the time-varying flux induced by an electric circuit, N is the number of turns of coils in the magnetic field, l_f and d_s are the width and the change in the length of the moving surface, respectively, and v is the velocity of the moving conductor. The minus sign in (2) shows that the induced current due to changing a magnetic field is in a direction such that it opposes the changes that produce it, which is Lenz's law. Note that in this paper a symbol E is used to indicate the induced voltage and a symbol V is used for the terminal voltage of a device. In a constant magnetic field and for a constant velocity of the moving conductor, the EMF can be changed by changing l_f in the magnetic field. This approach is taken here by keeping the rotor position fixed, and adjusting the overlap between the rotor and the stator by moving the stator relative to the rotor, as shown in Fig. 2. In effect, the difference in the overlap can be thought of as having different generators with varying lengths and the same width in series.

The one-phase equivalent circuit of a synchronous generator is shown in Fig. 3, where T_{pm} is the prime mover torque, T_{loss} are torque losses due to friction and wire winding, T is the electromagnetic torque, ω_{syn} is the synchronous speed, E_a is the induced voltage in the generator armature winding, X_s is the synchronous reactance, R_a is the armature resistance, I_a is the armature current, and V_a is the phasor sum of the total voltage and the voltage drop due to the armature resistance and the armature leakage reactance. At steady state, the mechanical torque from the prime mover should balance the electromagnetic torque provided by the generator and the torque losses: $T_{pm} = T + T_{loss}$. Multiplying this torque balance equation by ω_{syn} yields the power balance equation: $P_{pm} = P_g + P_{loss}$, where $P_{pm} = T_{pm}\omega_{syn}$ is the mechanical power supplied by the prime mover, $P_g = T\omega_{syn}$ is the electromagnetic power of the generator, and $P_{loss} = T_{loss}\omega_{syn}$ includes mechanical and electrical power losses. The true power and the electromagnetic torque of a synchronous generator with a cylindrical rotor are (Boldea 2006, Concordia 1951)

$$P_g = \frac{E_a V_a}{X_d}\sin\delta - \frac{V_a^2}{2}\left(\frac{1}{X_q} - \frac{1}{X_d}\right)\sin 2\delta \tag{3}$$

$$T = \frac{P_g}{\omega_{syn}} = \frac{E_a V_a}{\omega_{syn} X_d}\sin\delta + \frac{V_a^2}{2\omega_{syn}}\left(\frac{1}{X_q} - \frac{1}{X_d}\right)\sin 2\delta \tag{4}$$

respectively, where E_a and δ are the magnitude and the load angle of the induced voltage, respectively, V_a is the terminal voltage, Z_s is the synchronous impedance, X_q and X_d are the quadratic-axis and direct-axis synchronous reactance, respectively, and θ_s is the phase angle of the synchronous impedance.

If the effective armature resistance is neglected ($R \approx 0$), the magnitude of the synchronous impedance becomes that of the synchronous reactance ($|Z_s| = |X_s|$). The real power and the electromagnetic torque with $\theta_s = 90^\circ$ for a round-rotor machine with a uniform air gap ($X_q = X_d = X_s$) per phase can be simplified to

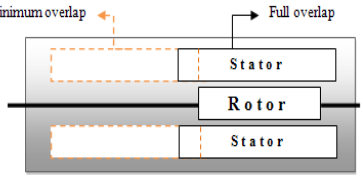

Fig. 2 Schematic of a VEG with a movable stator over the rotor at minimum and full overlap conditions

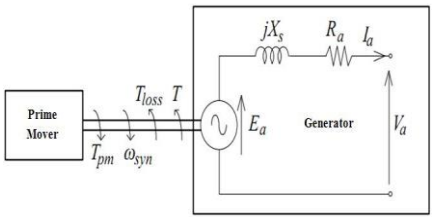

Fig. 3 Equivalent circuit of a synchronous generator

$$P_g = \frac{E_a V_a}{X_s}\sin\delta = P_{\max}\sin\delta \tag{5}$$

$$T = \frac{P_g}{\omega_{syn}} = \frac{E_a V_a}{\omega_{syn} X_s}\sin\delta \tag{6}$$

respectively. The load angle can be estimated using the phasor diagram (Idzotic *et al*. 2004)

$$\delta = \arctan\left(\frac{I_a X_S P - I_a R_s Q}{V_a S + I_a X_S Q + I_a R_s P}\right) \tag{7}$$

where P is the true power, Q is the reactance power, and S is the apparent power. The ratio of the generated power at any input speed to that at the minimum running speed of a regular generator with a fixed terminal voltage and a specific synchronous speed is

$$\frac{P_{gi}}{P_{g\min}} = \frac{E_i}{E_{\min}} \frac{\sin\left(\arctan\left(\frac{I_{ai}X_{Si}P - I_{ai}R_{si}Q}{V_{ai}S + I_{ai}X_{Si}Q + I_{ai}R_{si}P}\right)\right)}{\sin\left(\arctan\left(\frac{I_{a\min}X_{S\min}P - I_{a\min}R_{S\min}Q}{V_{a\min}S + I_{a\min}X_{S\min}Q + I_{a\min}R_{S\min}P}\right)\right)} \frac{X_{S\min}}{X_{si}} \tag{8}$$

where the subscript i in P_{gi}, E_i, I_i, X_{Si}, and R_i denotes any input speed. Using power relations among the true, apparent, and reactant powers and substituting (2) into (8) for the induced voltage in the generator with a constant width of the magnetic field, one has

$$\frac{P_{gi}}{P_{g\min}} = \frac{A_i}{A_{\min}} \frac{\sin\left(\arctan\left(\frac{X_{Si}}{R_L}\right)\right)}{\sin\left(\arctan\left(\frac{X_{S\min}}{R_L}\right)\right)} \frac{X_{S\min}}{X_{Si}} \tag{9}$$

where A_i and $A_{\min}$ are effective moving surface areas at any input speed and the minimum running speed of the regular generator, respectively, and R_L is the load resistance. The generator output power is a function of the input power; for small time intervals at which the generator output power linearly changes with the input power, the ratio of the overlap between the rotor and the stator at any speed to that at the minimum running speed can be obtained from

$$\frac{A_i}{A_{\min}} = \frac{P_i}{P_{\min}} \frac{\sin\left(\arctan\left(\frac{X_{S\min}}{R_L}\right)\right)}{\sin\left(\arctan\left(\frac{X_{Si}}{R_L}\right)\right)} \frac{X_{Si}}{X_{S\min}} \tag{10}$$

where P_i and $P_{\min}$ are the input powers at any speed and the minimum running speed, respectively. In a wind turbine, the rotor power at the minimum running speed (i.e., the cut-in speed) $U_{\min}$ is (Manwell *et al*. 2009)

$$P_{r_{\min}} = \frac{1}{2}\eta_{mech_{\min}} Cp_{\min}\rho A_r U_{\min}^3 \tag{11}$$

where $P_{r_{\min}}$ is the minimum output rotor power of a wind turbine at the cut-in speed, $\eta_{mech_{\min}}$ and $C_{P_{\min}}$ are the mechanical efficiency and the power coefficient at the cut-in speed, respectively, ρ is the air density, and A_r is the rotor swept area. Hence for a wind turbine application, the first ratio on the right-hand side of (10) is the ratio of the rotor power at any wind speed to that at the cut-in speed

$$\frac{P_{ri}}{P_{r_{\min}}} = \frac{\eta_{mechi} Cp_i U_i^3}{\eta_{mech_{\min}} Cp_{\min} U_{\min}^3} \tag{12}$$

and the other two ratios are obtained from generator specifications.

3. Design procedure for the VEG

An experimental test stand is designed and fabricated, which includes three main steps: modifying a regular generator to a VEG with an adjustable overlap between the rotor and the stator, designing an active control system for automatic overlap adjustment, and developing a test procedure to provide required data for validating the VEG concept.

3.1 Design and fabrication of the VEG

Fig. 4 shows the schematic of a VEG test stand modeled in SolidWorks. The electric motor is mounted by clamshell style mounting brackets that constrain it at two locations. The output shaft of the electric motor and the generator shaft are attached by a love-joy shaft coupler. A regular generator is modified to have an adjustable overlap between the rotor and the stator. A movable carrier is designed to hold the generator stator and allow it to have an axial motion along the generator rotor axis, which adjusts the overlap ratio from 0% to 100%. It is supported with four stainless steel rods parallel to the generator rotor axis and its axial movement is achieved through an ACME rod that transfers rotational motion to axial motion, as explained below.

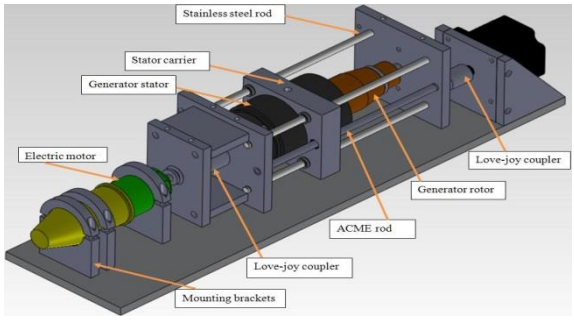

Fig. 4 Schematic of a VEG test stand modeled in SolidWorks

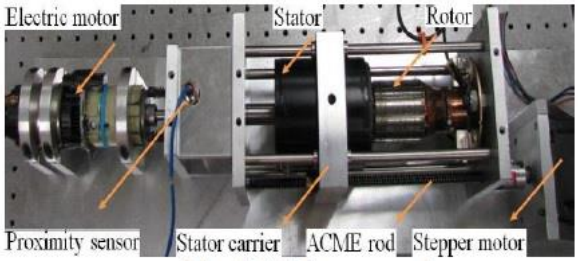

Fig. 5 VEG test stand

Fig. 5 shows the final VEG test stand. A 24 V direct-current (DC) motor with an output power of 700 W and a wide range of rotational speeds, with the maximum rotational speed of 19000 RPM used to model the output rotor power (Kendrick 2012). A 12 V synchronous DC generator is modified to have a VEG feature. Since the air gap between the rotor and the stator has a major impact on the generator output, careful attention to machining tolerance and adjustment of the moving stator carrier throughout the range of motion of the stator is required. Accomplishing this high precision task requires careful consideration of the alignment and balance of the system, with tolerance of 0.025 millimeter (1/1000 inch). To facilitate assembly, the stator is chilled in a refrigerator at a temperature of approximately 2.78˚C (37˚F), and the aluminum carrier is warmed using a heat gun to a temperature of approximately 65.56˚C (150˚F). This allows the assembly to be a nearly sliding fit, with some room to ensure that the two parts remain in alignment while cooling them to a snug interference fit. The stator carrier and all the plates and fixtures are made of 6061 aluminum to prevent any electrical interference. The ACME bushing is made of bronze to insulate the ACME rod from the stator frame. Both aluminum and bronze are non-magnetic metals. The stator carrier is mounted into the position in-line with the center of mass of the stator. Non-magnetic 316 stainless steel rods are used as the stator carrier supporters along its axial motion. An important feature to consider in designing the carrier and its supporting rods is the mass of the stator itself; it is critical that bending of the rods does not occur. For this test stand with a relatively low power yield, bending of the rods may be inconsequential. A custom-designed generator with an extended snout one-piece rotor can be used if necessary to allow the stator to move over the entire length of the rotor. If one uses a consumer off-the-shelf generator, it is necessary to fabricate an extension shaft. As the rotor size increases, the extension shaft and its interface with the rotor must be robust enough to prevent its bending and twisting while remaining stationary.

There are various methods for achieving a linear motion of the stator carrier; a linear actuator, an ACME rod, a timing pulley, and a hydraulic assembly can all be used to move the stator. A hydraulic assembly may be ideal but its design should allow compensation for environmental factors. An ACME rod with extremely high precision compared with a standard threaded rod is used to transfer rotational motion to axial motion. A high-precision low-cost Keling Technology stepper motor KL34H260-60-4A with an output torque of 3.284 Nm (465 oz-in), fixed to a mounting plate and connected to the ACME rod via a love-joy coupler, is used to control the position of the stator carrier at different rotor speeds. It is designed to have 200 steps per revolution for adjustment of the overlap between the rotor and the stator from 0% to 100% of the full overlap, which is equivalent to approximately 1.8 degrees of rotation per step. An Arduino Uno microcontroller provides a pulse-width-modulation (PWM) signal to control the transistors in the speed controller, allowing the voltage to flow through the controller. With pulse-width duration on the order of milliseconds, it is possible to achieve highly precise control of the output voltage. A curve-fitting method is used to obtain a fifth-order polynomial equation from experimental data to convert the PWM signal to the rotor speed in RPM

$$\omega = (1.91E-08)(S)^5 - (1.24E-04)(S)^4 + (3.21E-01)(S)^3 - (4.16E+02)(S)^2 + (2.69E+05)(S) - (6.96E+07) \quad (13)$$

where ω is the rotor speed and S is the PWM signal value. An IFI Robotic-Victor Pro 885 speed controller that operates at the 24 V nominal voltage is wired in series between the power supply and the motor, and processes the PWM signal. The power of the Victor Pro controller is supplied by a pair of Power-star 12-V 9-amp-hour sealed lead acid batteries. The batteries are wired in series to provide a total voltage of 24 V to the Victor Pro controller.

3.2 Active control system of the VEG

The current focus of the control system is on the steady-state response of the VEG; its nonlinearity may cause instability for different parameters, such as the desired output power or the desired overlap. Hence, in order to automatically control the VEG to generate a desired output power, the overlap between the rotor and the stator can be adjusted by an active control system that has two main parts: the data acquisition part (DAP) and the control (Ctrl) part, as shown in Fig. 6. The DAP is performed by using a precise proximity sensor to record the rotational speed, as shown in Fig. 5, and by calculating the corresponding desired output power that should be generated by the VEG. The Ctrl part that includes a feedback control system is to make the VEG generate the desired output power by adjusting the overlap between the rotor and the stator. The desired output power calculated in the DAP is the set point for the Ctrl part; the output power of the VEG is used as the feedback, and the difference between the desired and real output powers multiplied by a factor F, which will be discussed in Sec. 4, is the error between the real output power of the VEG and the desired one calculated in the DAP.

The control law for the Ctrl part is implemented using the National Instrument (NI) LabVIEW platform to design the control logic (Fig. 7), the SCB-68 data acquisition interface to monitor the output voltage of the generator, and the stepper motor as the actuator that is controlled by the UMI-7772 motion control interface. A proportional-integral (PI) controller with a proportional constant $P = 250$ and a unit integral constant converts the error to a signal that is

transmitted to the stepper motor controller to change the output power of the generator by adjusting the overlap between the rotor and the stator. More accurate output power reading in the DAP results in a faster and more precise overlap adjustment. This higher accuracy is required in reading the data and designing the control system, especially at low rotor speeds and for small overlap ratios between the rotor and the stator.

Overlap adjustment parameterization is developed based on the rotor speed of the generator. For a specific application of the VEG and the optimum output power of the generator, the desired output power can be discretely or continuously changed. For a hybrid vehicle application, there are discrete desired output powers at specific speeds for a required maximum and minimum electromagnetic torque as the vehicle decelerates and accelerates, respectively. For a wind turbine application with a continuously varied wind speed, the optimum output power at any rotor speed is required by continuously adjusting the overlap between the rotor and the stator.

3.3 Test procedure

The test procedure for acquiring the generator output voltage data for a complete assembly is outlined below:

1. Run the electric motor: this step simulates the actual arbitrary input power to the VEG that can be either a hybrid vehicle speed or the input wind speed of a wind turbine (Fig. 8).

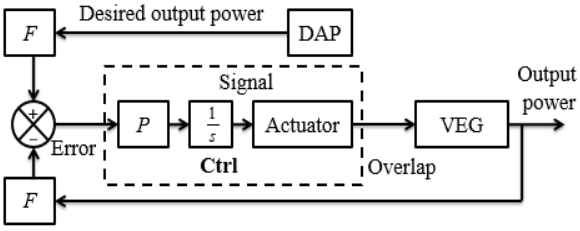

Fig. 6 Active control system of the VEG with two main parts: the DAP and the Ctrl part

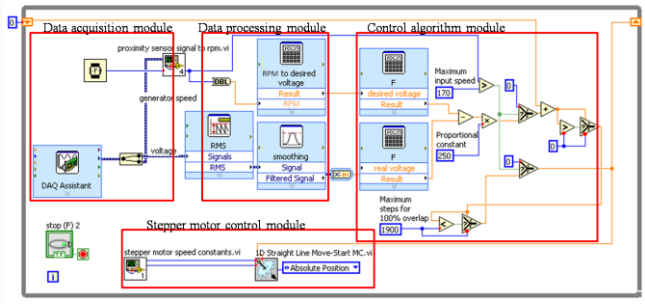

Fig. 7 NI LabVIEW block diagram for the active control system of the VEG

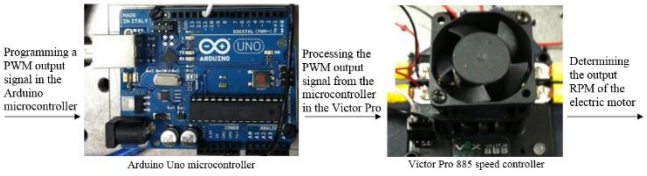

Fig. 8 Step one in the test procedure: running the electric motor

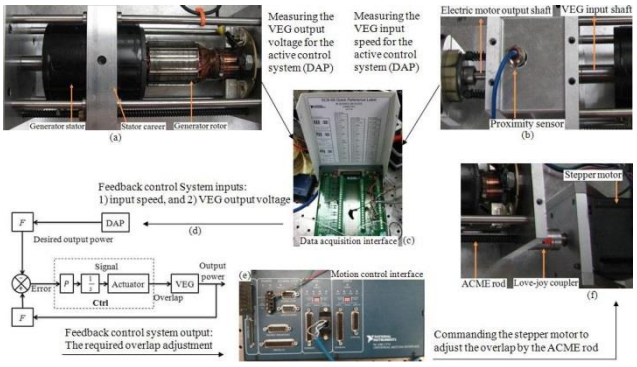

Fig. 9 Hardware for the test procedure: (a) the VEG, (b) the proximity sensor, (c) the data acquisition interface, (d) the control system, (e) the motion control interface, and (f) the stepper motor

2. Measure the VEG rotor speed: the actual output speed of the electric motor or the rotor speed of the VEG is measured by a precise proximity sensor attached to the top of the love-joy coupler between the electric motor and VEG shafts (Fig. 5). Connect the other end of the proximity sensor to the NI SCB-68 data acquisition interface shown in Fig. 9.
3. Connect large 6 kΩ resistors to terminals of the stator and the armature of the generator to eliminate high current values.
4. Connect the stepper motor to the NI UMI-7772 motion control interface (Fig. 9).
5. Set a desired output power as either a fixed or optimum value in the LabVIEW software, and run the active control system to adjust the overlap, as shown by the data processing module in Fig. 7.
6. Obtain the generator output voltage and speed through the data acquisition module in the LabVIEW software (Fig. 7), and monitor the generator input voltage and current by a digital multimeter.
7. Since the output load of the generator is a constant resistor, the root mean square (RMS) value of the generator output voltage is proportional to the output power in a sampling cycle. Hence, the RMS value in a sampling cycle is calculated in the data processing module to be the real output voltage, and four consecutive RMS values are averaged to smooth the output voltage. The desired output voltage is obtained using the generator speed in the data acquisition module.

8. The smoothed real output voltage and the desired output voltage are sent to the control algorithm module and the signal for actuating the stepper motor is generated in the stepper motor control module (Fig. 7).
9. Repeat the test for a range of PWM signals that cover a desired range of rotor speeds.
10. Unplug the Arduino microcontroller and turn off the system.

4. Results

4.1 Impact of the VEG on the rotor speed

Fig. 10 shows the normalized output voltage, denoted by V_a, versus the normalized rotor speed, denoted by Ω, from experimental data for different overlap ratios between the rotor and the stator, denoted by β, at steady state. The normalized output voltage and the normalized rotor speed are the output voltage divided by the maximum output voltage and the rotor speed divided by the maximum rotor speed, respectively; the output voltage decreases with the overlap. The first objective here is to determine whether the modified generator with an adjustable overlap between the rotor and the stator has less electromagnetic loss and can generate electricity at an input power lower than that at which the regular generator starts working. The normalized output voltage of a generator can be expressed by

$$V_a = \psi(\beta)\varphi(\Omega) \tag{14}$$

where Ψ and φ are a function of the overlap ratio and the normalized rotor speed, respectively. For constant overlap ratios shown in Fig. 10, a sixth-order polynomial function is used to establish the relation between the normalized output voltage and the normalized rotor speed

$$V_a = \psi(\beta)\varphi(\Omega) = \sum_{i=0}^{6} M_i(\beta)\Omega^i = \psi(\beta)\sum_{i=0}^{6} N_i \times \Omega^i \tag{15}$$

where $M_i(\beta)$ is the ith-order coefficient of V_a, which is a function of the overlap ratio, and N_i is the constant ith-order coefficient of $\varphi(\Omega)$. Each curve for a specific overlap ratio in Fig. 10 is fitted by a sixth-order polynomial function, and the ith-order coefficients for different overlap ratios can be determined, as shown in Fig. 11, which are used to fit the function $M_i(\beta)$ to describe the relation between the ith-order coefficient and the overlap ratio; however, it is difficult to find the functions $M_i(\beta)$ that can estimate the coefficients between the points calculated from the experimental data.

To resolve the above problem, the normalized output voltage can be expressed by functions of the overlap ratio at different rotor speeds. Logarithmic, polynomial, and exponential functions may be used to define the relation between the normalized output voltage and the overlap ratio. By some trials, one can find that polynomial and exponential functions cannot be used to express the normalized output voltage in (14). A logarithmic function can be used to express the normalized output voltage in (14) in terms of the overlap ratio and the rotor speed:

$$V_a = \varphi(\Omega)\psi(\beta) = l(\Omega)\ln(\beta) + b(\Omega) = \varphi(\Omega)(\ln(\beta) + \tilde{b}) \tag{16}$$

where $l(\Omega)$ and $b(\Omega)$ are coefficients of the logarithmic function and $\tilde{b}$ is a constant.

Each curve at a constant rotor speed is fitted by the logarithmic function and the coefficients $l(\Omega)$ and $b(\Omega)$ at different normalized rotor speeds are specified. By (19), $l(\Omega) = b(\Omega)$ and $b(\Omega) = \tilde{b} \times l(\Omega)$, which means that $\tilde{b}$ is the proportionality constant of $l(\Omega)$ and $b(\Omega)$. To find $\tilde{b}$, a fourth-order polynomial function is found to be the best choice to fit the curves of $l(\Omega)$ and $b(\Omega)$

$$l(\Omega) = -79.55\Omega^4 + 264.82\Omega^3 - 328.88\Omega^2 + 181.19\Omega - 37.22 \tag{17}$$

Table 1 Coefficients of the fourth-order polynomial functions of *l* and *b* and their ratios

Order	4th	3rd	2nd	1st	0th
$l(\Omega)$	-79.55	264.82	-328.86	181.19	-37.22
$b(\Omega)$	-231.61	771	-957.45	527.23	-108.20
Ratio	2.91	2.91	2.91	2.910	2.91

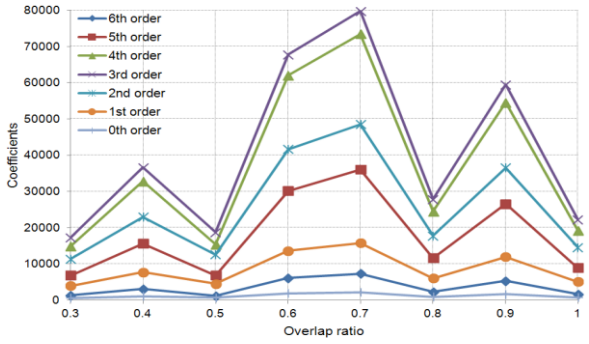

Fig. 10 Normalized output voltage versus the normalized rotor speed at different overlap ratios

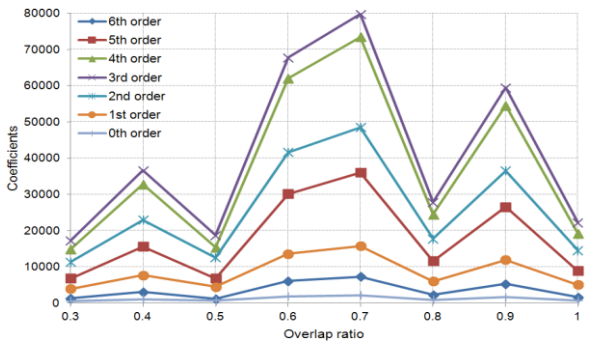

Fig. 11 Coefficients of the sixth-order polynomial function as functions of the overlap ratio

$$b(\Omega) = -231.60\Omega^4 + 771\Omega^3 - 957.45\Omega^2 + 527.23\Omega - 108.20 \quad (18)$$

Coefficients of $l(\Omega)$ and $b(\Omega)$ in (17) and (18), and their ratios are shown in Table 1. Since the ratio of the coefficients for each order of $l(\Omega)$ and $b(\Omega)$ is almost a constant, and the standard derivation of the ratios is 0.0017, the average of the ratios 2.91028 can be used as the proportionality constant

$$b(\Omega) = 2.91028 \times l(\Omega) \quad (19)$$

Substituting (21) into (18) yields

$$V_a = l(\Omega)[\ln \beta) + 2.91028] \quad (20)$$

Comparing (23) with (18) yields

$$\psi(\beta) = \ln(\beta) + 2.91028, \quad \varphi(\Omega) = l(\Omega) \quad (21)$$

Note that the expression of V_a in (20) has better accuracy at higher rotor speeds than very low ones due to relatively large noise and malfunction of the modified generator at very low ones.

The rotor speed and the output power are measured at any input power. Fig. 12 shows rotor speed variations at different input power levels due to decreasing the overlap between the rotor and the stator. The input power is indicated in a range from 1 to 10 to better generalize the methodology for different generators: 1 is the minimum input power that makes the rotor start spinning at the minimum overlap, 6 is the start-up power of the regular generator, and 8 to 10 are the powers that make the generator work as a regular generator following its power curve. The input power levels are obtained from the input PWM signals from the Arduino Uno microcontroller, and they increase with the input signal level. It is observed that at a constant input power, by decreasing the overlap between the rotor and the stator, the rotor speed is increased. Up to 12% increase in the rotor speed is achieved at low speeds by decreasing the overlap between the rotor and the stator. In addition, three speed ranges are observed in Fig. 12: the first range relates to the input speed lower than 110 RPM, the second one is a transition between the low and high input speeds, and the third one relates to the input speed higher than 160 RPM.

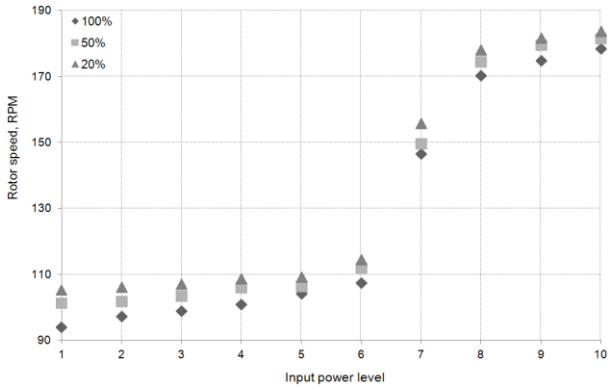

Fig. 12 Rotor speed variations at different input power levels and overlap ratios

Fig. 13 shows the changes in the normalized output power for different input power levels. While there is up to 12% increase in the rotor speed when the overlap between the rotor and the stator is at 20%, there is a significant reduction of up to 65% in the generator output power. In addition, there is a jump in the generator rotor speed from 110 RPM to 140 RPM when the input power level increases from the sixth to the seventh level. It is desirable to adjust the overlap ratio in order to generate the maximum power, while keeping the rotor spinning at a maximum speed. While theoretical analysis shows the possibility of increasing the rotor speed by decreasing the overlap ratio between the rotor and the stator to 20% or even lower and still making the generator work, the experimental results show that a more steady behavior and smoother changes of the generator output power are achieved at an overlap ratio larger than 50%.

There is a trade-off for the VEG to work at a smaller input power and have a stable and smooth output power; the optimum condition is obtained when the overlap ratio between the rotor and the stator is between 50% to 100% for the rotor speed less than 170 RPM, and the full overlap between the rotor and the stator is preferred for the rotor speed above 170 RPM. The three ranges of low, transition, and high output powers in Fig. 13 are similar to those in Fig. 12 for the rotor speed. Higher overlap ratios (more than 50%) between the rotor and the stator result in higher output powers at lower rotor speeds, and lower overlap ratios (less than 50%) result in lower output powers at higher rotor speeds. This can be employed in a hybrid vehicle to store a maximum power at the full overlap and have the minimum electromagnetic loss at a minimum overlap ratio. It can also be employed in a wind turbine to expand its operational range at low wind speeds; the VEG works as a regular generator as the wind speed increases.

4.2 Validation of the mathematical model

The mathematical model in Sec. 2 is checked against the experimental data for three overlap ratios of 100%, 50%, and 20% at different rotor speeds lower than 170 RPM. For a generator in a hybrid vehicle, a wind turbine, and so on, the overlap ratio can be obtained based on the generator specifications and the ratio of the input power at any input speed to that at the current minimum running speed of the generator. The overlap ratio between the rotor and the stator in (13) can be expressed by a polynomial function of degree n

$$\frac{A_i}{A_{\min}} = \frac{P_i}{P_{\min}} \begin{pmatrix} a_{i,1} & \cdots & a_{i,n} \end{pmatrix} \begin{bmatrix} Y^n \\ \vdots \\ 1 \end{bmatrix} = \frac{P_i}{P_{\min}} k_n \quad (22)$$

where A_i, P_i and $A_{\min}, P_{\min}$ are the effective moving surface area and the input power at any wind speed and those at the minimum running speed of the regular generator, respectively; the second and third terms in the middle expression correspond to the generator specification ratio, which is the polynomial k_n of degree n on the right-hand side, in which n and the coefficients $a_{i,j}$ depend on

the type of the generator and the test conditions, and Y depends on the generator specifications and the rotor speed. The generator specification ratio k_n can be obtained through a set of tests for a specific range of input powers and a specific overlap ratio, and modified for other input powers and overlap ratios. For different input powers and rotor speeds lower than 170 RPM at 100%, 50%, and 20% overlap ratios, k_n are best obtained from the experimental data using a third-, a second-, and a first-order polynomial, respectively

$$k_{n(100\%\text{overlap})} = -0.0021Y^3 + 0.0196Y^2 - 0.0767Y + 1.0588 \quad (23)$$

The changes in the k_n values increase with the input power and the overlap ratio. For any input power with the rotor speed lower than 170 RPM, substituting (26)-(28) into (25), one can find an area ratio of 1, 0.5, and 0.2, respectively. Table 2 shows comparison of the area ratios from the experiment and the mathematical model at different input power levels. Note that the rotor speeds are measured with an accuracy of ± 3 RPM for the calculated values in Table 2. There is a very good correlation between the results from the experiment and the mathematical model for different input powers; the maximum errors for the 100%, 50%, and 20% overlap ratios do not exceed 2%. As the rotor speed reaches the minimum running speed of the regular generator, which is 170 RPM in this study, the modified generator works as the regular one with a full overlap between the rotor and the stator and follows the regular power curve.

4.4 Active control system

The controlled signal in the control system is the output power fed back from the VEG, and the error between the feedback and desired output powers are used to generate the control signal. In Fig. 6, there are two identical blocks *F*, which are called conditioning factors, before the differential node to obtain the error. The conditioning factors are used to condition the feedback and desired output powers. If the functions of the conditioning factors are unit, the error is exactly the difference between the output powers. If the functions of the conditioning factors are functions other than the unit function, the error is the difference between the conditioned feedback and desired output powers, which is called the conditioned error.

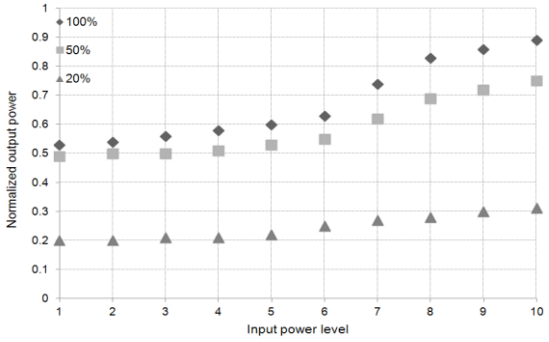

Fig. 13 Normalized output power at different input power levels and overlap ratios

Table 2 Comparison of the area ratios from the experiment and the mathematical model at 100%, 50%, and 20% overlap

100% overlap		
Input power level	Experiment	Mathematical model
1	1	0.9996
2	1	1.0020
3	1	0.9979
4	1	1.0011
5	1	1.0004
6	1	0.9996
50% overlap		
Input power level	Experiment	Mathematical model
1	0.5	0.4998
2	0.5	0.4994
3	0.5	0.5109
4	0.5	0.5040
5	0.5	0.4939
6	0.5	0.4809
20% overlap		
Input power level	Experiment	Mathematical model
1	0.2	0.2013
2	0.2	0.1984
3	0.2	0.1955
4	0.2	0.1926
5	0.2	0.1897
6	0.2	0.1809

When the conditioning factor is unit, the discretely changed, normalized feedback and desired output powers of the VEG, which are the feedback and desired output powers divided by those at the full overlap, respectively, are shown in Fig. 14. When the desired output power is larger than 0.5, the real output power is stable (Fig. 14). When the normalized desired output power is 0.5 and the overlap ratio is about 75%, the normalized output power of the VEG becomes stable after a transient; there are small oscillations after the transients since the regular generator is modified to allow for overlap adjustment. When the normalized desired output power is less than 0.4 and the overlap ratio is less than 20%, the normalized output power of the VEG is unstable. The instability results from the nonlinear relation between the output power and the overlap ratio, as shown in Fig. 15. If the overlap ratio gets smaller, the changing rate of the output power with the overlap ratio becomes steeper, and the output power at a small overlap ratio is more sensitive to noise than that at a large overlap ratio. The sensitivity of the output power to the overlap ratio is the proportional constant in the control system; a large proportional constant for a small overlap ratio pushes the VEG towards the unstable region and it is more sensitive to noise. In order to make the VEG stable at every overlap ratio, the conditioning factor *F* is used to change the varied sensitivity to a relatively small constant value, which results in a more robust control system to noise. The relation between the output power and the overlap ratio in Fig. 15 is used to fit a function for the conditioning factor

$$F = 1.633P_g^{\,2} - 0.914P_g + 0.2347 \quad (26)$$

where P_g is the normalized fedback or desired output power. The conditioned output power is the output power multiplied by the conditioning factor, and the relation between the conditioned output power and the overlap ratio is also shown in Fig. 15. Eq. (26) shows that when the normalized feedback or the desired output power is small at a small overlap ratio, the slope of the conditioning factor is small, the sensitivity of the conditioned output power is small, and the output of the VEG is stable at every overlap ratio, as shown in Fig. 16.

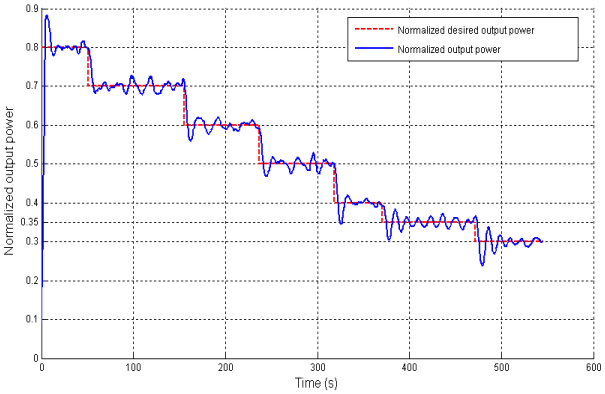

Fig. 16 Output power of the VEG with the conditioning factor in (26), which is stable at every overlap ratio

5. Conclusions

A novel VEG, which is a modified generator with an adjustable overlap between the rotor and the stator, is developed. It has a broad range of applications in hybrid vehicles, wind turbines, water turbines, and similar technologies. A mathematical model of the VEG is derived, and a prototype, which includes a 12-V synchronous DC generator with an adjustable overlap between the rotor and the stator, a 700-W electric motor as the prime mover, and a stepper motor as the actuator for an active control system of the VEG, is designed and fabricated.

A logarithmic function is found to be the best one for describing the relation between the output power of the VEG at different overlap ratios and rotor speeds. By reducing the overlap between the rotor and the stator, reduced torque loss and an increased rotor speed of up to 12% are achieved. However, significant decrease of the output power of up to 65% is observed at the 20% overlap ratio. There is a very good correlation between the results from the experiment and the mathematical model, and the maximum error does not exceed 2%.

A simple and robust active control system is developed for different applications with discretely and continuously changed, desired output powers. Due to the nonlinear relation between the overlap ratio and the output power, a conditioning factor, which is a function of the output power, is determined to guarantee stability of the control system. The VEG can expand the operational range of a wind turbine or a water turbine, especially in low-speed regions with high-speed fluctuations.

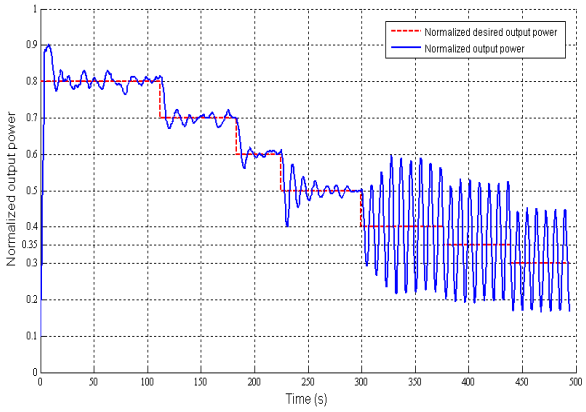

Fig. 14 Output power of the VEG, which is stable when the desired normalized output power is larger than 0.5 and unstable when the desired normalized output power is less than 0.4

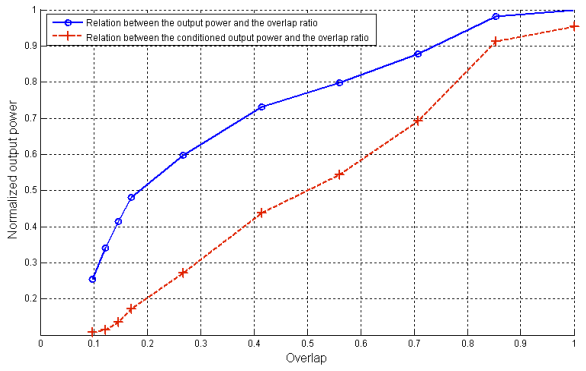

Fig. 15 Unconditioned and conditioned, normalized output powers of the VEG versus the overlap ratio

Acknowledgments

This work was supported by the Maryland Industrial Partnership program and the National Science Foundation under Grant No. CMMI-1335397.

References

Advanced Wind Turbine Drivetrain Concepts (2010), U.S. Dept. of Energy, DOE/GO-102010-3198, USA.

Al-Adsani, A.S. and Schofield, N. (2009), "Hybrid permanent magnet generators for electric vehicle applications", *Proceedings of the IEEE International Electric Machines and Drives Conference*, May 3-6, Miami, USA, 1754-1761.

Automotive World (2013), Allison Transmission to Unveil Fully-Automatic Hybrid for Commercial Vehicles. Available: http://www.automotiveworld.com/news-releases/allison-

transmission-to-unveil-fully-automatic-hybrid-for-commercial-vehicles/

Baumann, B.M., Washington, G., Glenn, B.C. and Rizzoni, G. (2000), "Mechatronic design and control of hybrid electric vehicles", *IEEE/ASME Trans. Mechatron.*, 5(1), 58-72.

Bishop, R.S. (2008), *Mechatronic Systems, Sensors, And Actuators*, 2nd Ed., CRC press, ch. 21.

Boldea, I. (2006), "Synchronous Generators", 1st Ed., *FL*, CRC press.

Bywaters, G., John, V., Lynch, J., Mattila, P., Norton, G., Stowell, J., Salata, M., Labath, O., Chertok, A. and Hablanian, D. (2004), "Northern power systems windPACT drive train alternative design study report," National Renewable Energy Laboratory (NREL), Golden, CO, Rep. NREL/SR-500-35524.

Caricchi, F., Crescimbini, F., Giulii Capponi, F. and Solero, L. (2001), "Permanent-magnet, direct-drive, starter/alternator machine with flux linkage for constant-power operation over extremely wide speed range", *Proceedings of the Ind. Appl. Conference, 36th IAS Annual Meeting*, October.

Chau, K.T., Li, Y.B., Jiang, J.Z. and Liu, C.H. (2006), "Design and analysis of a stator-doubly-fed doubly-salient permanent-magnet machine for automotive engines", *IEEE T. Magn.*, **42**(10), 3470-3472.

Chen, Y.C., Pillay, P. and Khan, A. (2005), "PM wind generator topologies", *IEEE T. Ind. Appl.*, **41**(6), 1619-1626.

Chen, Z., Guerrero, J.M. and Blaabjerg, F. (2009), "A review of the state of the art of power electronics for wind turbines", *IEEE T. Power Electr.*, **24**(8), 1859-1875.

Concordia, C. (1951), "Synchronous machines, theory and performance", 1st Ed., *London*, UK, Chapman and Hall.

Crescimbini, F., Di Napoli, A., Solero, L. and Caricchi, F. (2005), "Compact permanent-magnet generator for hybrid vehicle Applications", *IEEE T. Ind. Appl.*, **41**(5), 1168-1177.

Del Ferraro, L., Capponi, F.G., Terrigi, R., Caricchi, F. and Honorati, O. (2006), "Ironless axial flux PM machine with active mechanical flux weakening for automotive applications", *Proceedings of the Ind. Appl. Conference, 41th IAS Annual Meeting*, Oct. 08-12, Tampa, USA.

Deng, F.J. and Chen, Z. (2010), "Variable speed wind turbine based on multiple generators drive-train configuration", *Proceedings of the IEEE Innovative Smart Grid Technologies Conference Europe*, Oct. 11-13, , Gothenberg, Sweden.

Dubois, M. (2004), "Optimized permanent magnet generator topologies for direct drive wind turbines", Ph.D. dissertation, Delft University of Technology, Delft, NL.

Emadi, A., Rajashekara, K., Williamson, S.S. and Lukic, S.M. (2005), "Topologies overview of hybrid electric and fuel cell vehicular power system architectures and configurations", *IEEE T. Veh. Technol.*, **54**(3), 763-770.

Gaussens, B., De La Barriere, O., Hoang, E., Saint-Michel, J., Manfe, P., Lecrivine, M. and Gabsi, M. (2013), "Magnetic field solution in doubly slotted airgap of conventional and alternate field-excited switched-flux topologies", *IEEE T. Magn.*, **49**(9), 5083-5096.

Goudarzi, N. and Zhu, W.D. (2013), "A review on the development of the wind turbine generators across the world", *Int. J. Dynam. Control*, **1**(2), 192-202.

Goudarzi, N., Zhu, W.D. and Bahari, H. (2014), "An assessment of the potential of a novel ducted turbine for harvesting wind power", *J. Intel. Mat. Syst. Str.*, **26**(9), 1059-1070.

Goudarzi, N. and Zhu, W.D. (2013), "Offshore and onshore wind energy conversion: The potential of a novel multiple-generator drivetrain", *Key Eng. Mater.*, **569-570**, 644-651, Available: http://www.ttp.net/978-3-03785-796-0.html.

Goudarzi, N., Zhu, W.D. and Bowers, R. (2012), "Aerodynamic and electromagnetic analysis of a variable electromotive-force generator for a wind turbine", *Proceedings of the ASME International Mechanical Engineering Congress & Exposition*, Nov. 9-15, Houston, TX, USA.

Hau, E. (2006), "Wind turbines; fundamentals, technologies, application, economics", 2nd Ed., Berlin, Germany, Springer.

Idzotic, T., Erceg, G. and Sumina, D. (2004), "Synchronous generator load angle measurement and estimation", *Automatica*, **45**(3-4), 179-186.

Kendrick, P. (2012), "Development and Analysis of a Variable Electromotive Force Generator for Use in Wind Turbine Applications," M.S. Thesis, Dept. Mech. Eng, Univ. Maryland, Baltimore County, MD.

Lewis, C. and Muller, J. (2007), "A direct drive wind turbine HTS generator", *IEEE Power Eng. Soc. General Meeting*, June 24-28, Tampa, USA

Li, H., Chen, Z. and Polinder, H. (2006), "Research report on numerical evaluation of various variable speed wind generator systems", Inst. of Energy Techno., Aalborg Uni., Delft Uni. of Technol., Rep. D 1B2. b.3.

Manwell, J.F., McGowan, J.G. and Rogers, A.L. (2009), "Wind energy explained; Theory, design, and application", 2nd Ed., Wiltshire, UK, John Wiley & Sons.

Mbayed, R., Salloum, G., Vido, L., Monmasson, E. and Gabsi, M. (2012), "Hybrid excitation synchronous machine control in electric vehicle application with copper losses minimization", *Proceedings of the Power Electronics, Machines and Drives (PEMD), 6th IET International Conference on*, Bristol, UK, March.

Mikhail, A. (2011), "Distributed generation drivetrain for high torque wind turbine applications", Clipper Windpower Technol. Inc., Rep. CEC-500-2011-002.

Nasar, S.A. and Boldea, I. (1990), "Electric machines, steady-state Operation", Hemisphere Publishing Corp., ch. 2-4, 19-160.

Owen, R.L., Zhu, Z.Q., Wang, J.B., Stone, D.A. and Urquhart, I. (2011), "Review of variable-flux permanent magnet machines," *Proceedings of the Int. Conf. on Elec. Machines and Syst*., Aug. 20-23, Beijing, China.

Owen, R.L., Zhu, Z.Q., Wang, J.B., Stone, D.A. and Urquhart, I. (2011), "Mechanically adjusted variable-flux concept for switched-flux permanent-magnet machines", *Proceedings of the International Conference on Electrical Machines and Systems*, Aug. 20-23, Beijing, China.

Polinder, H., Pijl, F.F.A., De Vilder, G.J. and Tavner, P. (2006), "Comparison of direct-drive and geared generator concepts for wind turbine", *IEEE T. Eng. Conver.*, **21**(3), 725-733.

Rafiee, M., Siadatan, A. and Afjei, E. (2012), "Improving the hybrid electric vehicles efficiency, using Si0.7Ge0.3 and Bi2Te3 thermoelectric materials", *Proceedings of the 4th International Conference on Intelligent and Advanced Systems* (*ICIAS*), June 12-14, Kuala Lumpur, Malaysia.

Schiferl, R., Flory, A., Livoti, W.C. and Umans, S.D. (2008), "High-temperature superconducting synchronous motors: Economic issues for industrial applications", *IEEE T. Ind. Appl.*, **44**(5), 1376-1384.

Somayajula, D., Meintz, A. and Ferdowsi, M. (2009), "Designing efficient hybrid electric vehicles", *IEEE Veh. Technol. Mag.*, **4**(2), 65-72.

Variable Torque Motors LLC (2009), "Transit Applications of the Variable Torque Motors Parallel Hybrid Drive System", Fort Wayne, IN, 1-13.

Wentworth, S.M. (2005), "Fundamentals of electromagnetic with engineering applications", 1st Ed., *NJ, John Wiley & Sons*, Part I, 9-258.

Williamson, S.S., Wirasingha, S.G. and Emadi, A. (2006), "Comparative investigation of series and parallel hybrid electric drive trains for heavy-duty transit bus applications", *Proceedings of the IEEE Vehicle Power and Propulsion Conference*, Sep. 06-08, Windsor, UK.

Zepp, L.P. (2011), "Brushless permanent magnet motor/generator with axial rotor decoupling to eliminate magnet induced torque losses", U.S. Patent 7863789B2, Jan. 04.

Zhou, G., Miyazaki, T., Kawamat, S., Kaneko, D. and Hino, N. (2010), "Development of variable magnetic flux motor suitable for electric vehicle", *Proceedings of the International Power Electronic Conference*, June 21-24, Sapporo, Japan.